Membrane Water Treatment, *Vol. 9, No. 1 (2018) 53-62*
DOI: https://doi.org/10.12989/mwt.2018.9.1.053

Treatment of high-salinity wastewater after the resin regeneration using VMD

Junyu Gao[a], Manxiang Wang and Yanbin Yun[*]

School of Environmental Science and Engineering, Beijing Forestry University, No. 35 Qinghua East Road, Haidian District, Beijing, 100083, China

(Received March 2, 2017, Revised July 15, 2017, Accepted October 24, 2017)

Abstract. In this study, vacuum membrane distillation (VMD) was used to treat high-salinity wastewater (concentration about 17%) discharged by chlor-alkali plant after resin regeneration. The feasibility of VMD for the treatment of real saline wastewater by using Polyvinylidene fluoride (PVDF) microporous plate membrane with a pore diameter of 0.2 μm was investigated. The effects of critical operating parameters such as feed temperature, velocity, vacuum degree and concentration on the permeate water flux were analyzed. Numerical simulation was used to predict the flux and the obtained results were in good agreement with the experimental data.The results showed that an increase in the operating conditions could greatly promote the permeate water flux which in turn decreased with an increase in the concentration. When the concentration varied from 17 to 25%, the permeate water flux dropped marginally with time indicating that the concentration was not sensitive to the decrease in permeate water flux. The permeate water flux decreased sharply until zero due to the membrane fouling resistance as the concentration varied from 25 to 26%. However, the conductivity of the produced water was well maintained and the average value was measured to be 4.98 μs/cm. Furthermore, a salt rejection of more than 99.99% was achieved. Overall, the outcome of this investigation clearly indicates that VMD has the potential for treating high-salinity wastewater.

Keywords: vacuum membrane distillation (VMD); high-salinity wastewater; operating conditions; concentration; membrane fouling; permeate flux

1. Introduction

The chlor-alkali industry is a crucial raw material industry that produces sodium hydroxide, chlorine and hydrogen via electrolysis of sodium chloride solution (Han *et al.* 2014). Since the metal ions of salt solution can corrode the metal tank and thus it necessitates its treatment. In chlor-alkali plant, the chelating resin is used to treat the brine solution containing metal ions. After saturation of chelating resin, high-salinity wastewater (the main component is NaCl and the concentration is about 17%) was produced after resin regeneration through acid exchange. It is to be noted that if the untreated wastewater is discharged directly, it would lead to severe damage of soil, plant, aquatic life, surface and groundwater etc. (Zhao *et al.* 2011). The traditionally followed biological technologies (Rania *et al.* 2016) facing difficulty to treat high-salinity wastewater due to the inhibition and/or due to the toxicity of salinity. The two major physical and chemical separation techniques that are currently used include thermal and membrane processes which are in specific widely followed in the petrochemical industries. However, the energy consumption of thermal technology is similar to multi-effect distillation (MED) or multi-stage flash distillation (MSF) processes i.e., approximately 40 kWh/m^3 (Khayet *et al.* 2003, Martínez-Díez *et al.* 1999, Obaidani *et al.* 2008, Avlonitis *et al.* 2003). In case of membrane desalination technology, reverse osmosis (RO) is well recognized as the most convenient which is the leading technology among the membrane desalination processes with 2/3 of the contracted capacity (Yan *et al.* 2017, Ducrotoy *et al.* 2008). Nevertheless, contrary to other membrane technologies such as membrane distillation (MD), a high-salt concentration cannot be achieved in RO.

MD is a newly emerging membrane-based desalination technique which combines the advantages of thermal distillation and membrane separation technologies. It is considered as a thermally-driven separation process for removing water vapor and volatiles from a warm aqueous feed solution at a temperature lower than 100℃ (Amali *et al.* 2004, Li *et al.* 2008). Therefore, MD is expected to be a cost-effective membrane separation process. In addition, one of the most important advantages of MD is that it is not limited by the well-known concentration polarization phenomenon thereby it can handle highly concentrated aqueous solutions. Recently, MD has attracted significant attention as a potential technology for the desalination of highly saline aqueous water and for the treatment of brines (Geng *et al.* 2014, Singh *et al.* 2012, Alkhudhiri *et al.* 2013, Edwie *et al.* 2013).

A large number of investigations report on the influence of higher salt concentrations on the permeate flux. Martinez (2004) reported that in direct contact membrane distillation (DCMD) the water flux decreased with an increase in the feed concentration which is associated with an increase in the feed solution viscosity and a decrease in water activity

*Corresponding author, Professor
E-mail: yunyanbin@bjfu.edu.cn
[a]Student
E-mail: 1113109804@qq.com

ISSN: 2005-8624 (Print), 2092-7037 (Online)

(Guan *et al.* 2015, Hickenbottom *et al.* 2014). Also, Yun *et al.* (2006) reported that water fluxes began to decrease sharply when the concentration of NaCl solution was close to saturation. After saturation, water fluxes approached a steady state gradually. Sanmartino *et al*. (2016) utilized a range of commercial membranes to test the desalination of highly saline water by air gap membrane distillation (AGMD), where they noted a higher feed temperature which is beneficial in improving the thermal efficiency of AGMD process. In addition, the effect of concentration polarization on the decline of permeate flux could be neglected as compared to the temperature polarization effect regardless of the feed concentration. When saline water is treated through vacuum membrane distillation (VMD), the water flux decreased by about 20-35% with an increase in the salt concentration from 1 to 3 mol/L (Wirth *et al.* 2002, Safavi *et al.* 2009, Naidu *et al.* 2014).

Compared to other categories of MD, VMD received a great deal of attention by many investigators as a low-cost, highly-efficient and energy-saving technique to wastewater treatment processes (2008). In the recent years, there are many applications that utilize VMD such as the concentration of fruit juices and lignocellulosic hydrolyzates (Diban *et al.* 2009, Zhang *et al.* 2015) and the treatment of wastewater (Akdemir *et al.*2009, Garcia-Castello *et al.* 2010, Dao *et al.* 2016). However, there are few studies dealing with the treatment of real high-salinity wastewater. Zhang *et al*. (2016) investigated the feasibility of VMD for the treatment of real high saline wastewater, where they achieved an ultrahigh water flux of 30.4 kg/(m^2·h) with a salt rejection rate of 99.8%. But the treatment of wastewater where the concentration is approaching to 17% has not been studied by VMD directly. In addition, there is no study on the prediction of permeate water flux with numerical simulation in real high-salinity wastewater.

Based on this, this investigation aims to explore the feasibility of industrial application of VMD in the treatment of real high-salinity wastewater after resin regeneration (concentration about 17%). For this purpose, PVDF microporous plate membrane was utilized and the simulated wastewater was used as the feed. The effect of different operating conditions such as the feed temperature, flow velocity and vacuum degree and concentration on the permeate water flux was investigated and the numerical simulation was adopted to describe the real high-salinity wastewater in this VMD process. Following this, the effects of three operating conditions on the concentration polarization and temperature polarization were analyzed by simulations. The obtained results from this study would be helpful in the application of treating real high-salinity wastewater using VMD in the near future.

2. Theoretical heat and mass transfer models in saline water

In the VMD process, the hydrophobic microporous membrane separates the membrane module into two channels; evaporation takes place at the hot feed side and transferred through the pores of membrane while the condensation takes place at the vacuum side. Therefore, heat and mass transfer occur simultaneously and are generally considered to be the key parameters determining the overall performance.

2.1 Mass transfer model

The mass transfer can be given based on Fick's law as

$$J = K\Delta P = K(P_{fm} - P_{pm}) \tag{1}$$

where J is the water flux through the membrane, and K is the membrane mass transfer coefficient. The vapor pressure difference (ΔP) is the driving force generated by the temperature difference of the feed membrane surface (T_{fm}) and the permeate across the membrane (T_{pm}). The vapor pressure of the feed membrane surface (P_{fm}) is affected by the concentration of saline water which could be calculated by the following Eq. (2) (Sereno *et al.* 2011)

$$P_{fm} = x_s \gamma_{water} p_s \tag{2}$$

$$P_s = \exp(23.1964 - \frac{3816.44}{T_{fm} - 46.13}) \tag{3}$$

where, x_s is the molar ratio of water in the feed, γ_w is the activity coefficient of water in the saline water, and p_s is the saturated water vapor pressure on the vapor-liquid interface. In aqueous NaCl solution, γ_w could be solved by the following Eq. (4) (Schofield *et al.* 1987)

$$\gamma_{water} = 1 - 0.5x_{NaCl} - 10x^2_{NaCl} \tag{4}$$

P_{pm} is the absolute vapor pressure on the vacuum side which can be calculated by the following Eq. (5)

$$P_{pm} = P - P_v \tag{5}$$

where P is the atmospheric pressure and P_v is the vacuum degree at the vacuum side.

Transport mechanisms for mass transfer across the membrane depend on Knudsen number (Kn). Kn is defined as the ratio of the mean free path of water vapor molecules to the pore diameter of membrane. In fact, three diffusion models are well known in most of the theoretical studies related to membrane distillation which are Knudsen diffusion, Molecular diffusion and Poiseuille flow. Knudsen diffusion is commonly considered by most of the researchers, whereas Molecular diffusion is usually not considered when VMD is used. Numerous reports describe on the diffusion of molecules in the pores as Poiseuille flow–Knudsen diffusion. In this study, the pore diameter of PVDF membrane was 0.2 μm. The mean free path of water vapor molecules varies between 2.8 and 3.4 μm with the temperatures in the range between 30℃ and 65℃ which implies that Kn varies from 14 to 17 (Mengual 2004). Based on Dusty Gas Model (DGM), in this work, the combination of Poiseuille flow-Knudsen diffusion was applied to the molecular diffusion model. Thus, Poiseuille flow-Knudsen diffusion can be represented by the following Eq. (6)

$$K = 1.064\frac{\varepsilon \mathrm{r}}{\tau\delta}\left(\frac{M}{RT_{\mathrm{avg}}}\right)^{0.5} + \frac{\varepsilon^2 \mathrm{r}\mathrm{P}_{\mathrm{avg}}}{8\tau\delta\mu RT_{\mathrm{avg}}} \quad (6)$$

where ε, r, τ, μ and δ are the porosity, radius of pore size, pore tortuosity, viscosity and the thickness of membrane; K is the Knudsen diffusion coefficient; M is the molecular mass of water; R is the gas constant; T_{avg} is the average membrane temperature between membrane at the feed and vacuum sides; P_{avg} is the average pressure in the membrane hole.

In saline water, a reduction in the water flux occurs with an increase in the solute concentration in the feed. This is mainly due to the presence of solute which reduces the partial pressure of water vapor thereby reducing the driving force at the feed side. The rate of volatility of water vapor on the membrane surface is faster than the diffusion rate of solute in the feed side and the existence of the boundary layer induced the concentration on the membrane surface to become larger than the concentration in the feed side which is referred as concentration polarization phenomenon. Concentration polarization may increase the overall resistance to mass transfer and is the main cause for the decrease in the water flux. The solute concentration on the hot side of the membrane surface can be calculated by the following Eq. (7)

$$c_{fm} = c_f \exp(J/\rho k_s) \quad (7)$$

where c_{fm} is the solute concentration on the hot membrane surface, c_f is the solute concentration on the hot feed, and k_s is the solute mass transfer coefficient. The value of k_s can be evaluated by the following Graetz-Leveque Eq. (8) (Martinez 2000)

$$Sh = 1.86(\mathrm{Re}\, Sc\frac{d_h}{L})^{0.33} \quad (8)$$

where d_h is the characteristic length, L is the channel length, Re and Sc are Reynolds and Sherwood numbers respectively as represented by the following Eqs. (9) and (10).

$$Sh = k_s d_h / D \quad (9)$$

$$\mathrm{Re} = \frac{d_h v\rho}{\mu} \quad (10)$$

$$Sc = \mu/\rho D \quad (11)$$

where, v, ρ and D are the velocity, density, and the diffusion coefficient of the solute, respectively. Based on the above equations, the concentration polarization coefficient (CPC) can be calculated by the following Eq. (12)

$$CPC = c_{fm} / c_f \quad (12)$$

2.2 Heat transfer model

Heat transfer processes can be divided into three steps: (1) heat (Q_b) transferring from the hot feed across the heat boundary layer; (2) the latent heat of vaporization (Q_m) from the liquid phase to gas phase; (3) heat (Q_c) passing through the membrane by heat conduction. While the conducted heat (Q_c) loss can be ignored because of high vacuum in the membrane pores and low conductivity of membrane material. According to the law of conservation of energy, the heat from the hot feed across the heat boundary layer is equal to the latent heat of vaporization as represented by the following Eqs. (13)-(15).

$$Q_b = h_f(T_f - T_{fm}) \quad (13)$$

$$Q_m = J\Delta H \quad (14)$$

$$Q_b = Q_m \quad (15)$$

where h_f is the heat transfer coefficient at the liquid boundary layer, T_f is the temperature of the feed. ΔH is the latent heat of evaporation at a temperature $T_{f\,\mathrm{m}}$ which can be calculated via Eq. (16) (Tomaszewska 1993)

$$\Delta H = 2258.4 + 2.47 \times (373.15 - T_{fm}) \quad (16)$$

The heat transfer coefficient, h_f can be estimated by the following known empirical correlation (Eq. (17))

$$h_f = \frac{Nu\mu}{d_h} \quad (17)$$

Nu can be obtained by the following Graetz-Leveque Eq. (18) (Martinez *et al.* 2000)

$$Nu = 1.86(\mathrm{Re}\,\mathrm{Pr}\frac{d_h}{L})^{0.33} \quad (18)$$

where Pr is the Prandtl number which is given as follows (Eq. (19))

$$\mathrm{Pr} = \frac{C_p\mu}{k} \quad (19)$$

where C_p and k are the specific heat and thermal conductivity of the liquid, respectively. Similar to concentration polarization, the temperature polarization can enhance the heat transfer resistance which is inevitable. In the VMD process, temperature polarization coefficient (TPC) refers to the ratio of the temperature on the membrane surface to the temperature in the feed which is simply defined as

$$TPC = T_{fm} / T_f \quad (20)$$

However, there is little or essentially no concentration and temperature polarization on the permeate side as the water vapor is quickly taken away in the VMD process.

It is difficult to calculate the results directly because of the complex nature. The procedure of calculations is shown in Fig. 1. The software visual studio with language C# was used in this work. In order to simplify the simulation, at first, the temperature on the membrane surface is assumed to be the temperature in the feed. Then, a water flux value is assumed and the final result including T_{fm}, J, TPC and CPC etc. have been obtained by iterative operation.

3. Materials and methods

3.1 Membrane and membrane module

The PVDF microporous plate membrane was obtained from EMD Millipore Corporation and was used in the VMD configurations. The characteristics of the employed membrane have been listed in Table 1. The plate membrane module was self-designed (Fig. 2). The housing side (length×width×height) of the membrane module was 15 cm×7.5 cm×5 cm. In this module, the hydrophobic microporous membrane separates the membrane module into two channels; where one side of the membrane is in contact with the hot feed and the permeate product is removed from the other side of the membrane.

Table 1 Characteristics of membrane

Parameter	Units	Values
Average pore radius	μm	0.20
Porosity	%	80
Membrane thickness	mm	0.125
Contact angle	°	122.6
Effective membrane area	cm^2	40

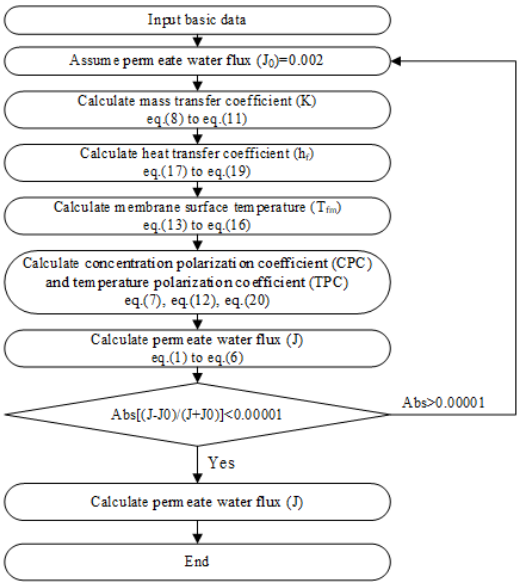

Fig. 1 The procedure of calculation

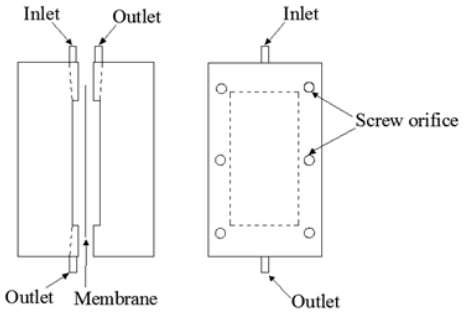

Fig. 2 Membrane module (left: cutaway view; right: ichnography of module)

Table 2 Components of the wastewater

Component	Units	Value
NaCl	g/L	200
Ca^{2+}	ppm	5
Mg^{2+}	ppm	3
Al^{3+}	ppm	100
Sr^{2+}	ppm	59
Si	ppm	200
IO^{3-}	ppm	600

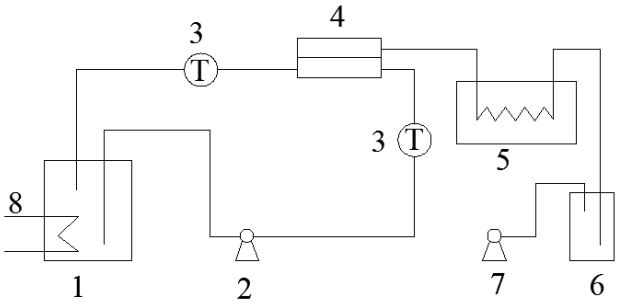

1 feed reservoir; 2 peristaltic pump; 3 temperature meter; 4 membrane module; 5 chiller; 6 permeate collection tank; 7 vacuum pump; 8 heater

Fig. 3 Schematic diagram of the VMD process

3.2 Simulated wastewater

The high-salinity wastewater was produced after resin regeneration and the wastewater was used for simulations. The components of wastewater have been given in Table 2. The simulated wastewater was pretreated by adjusting the pH before usage as feed in the VMD process. The purpose is to remove the influence of other metal ions depositing on the membrane surface.

3.3 Experimental set-up and procedures

The experimental set-up used in this study is shown in Fig. 3. There are two processes in the installation of VMD which are the feed cycle and vapor flowing processes. While the membrane module is the most important part which combines the two processes in the VMD operation. In this experiment, the feed was first heated in the feed reservoir, and then the hot feed was made to flow at a constant velocity through the rubber piping using a peristaltic pump. The hot feed into the flat membrane module contacts with PVDF microporous hydrophobic membrane. Evaporation of water occurs on the membrane surface due to heat transfer from the feed to the membrane surface. Then, the hot feed is cycled by the peristaltic pump to the feed reservoir. Temperatures were measured in or out of the membrane module. In the vapor flow process, the diffusion of water vapor through the membrane pores to the permeate side was induced by the vacuum pump. The water vapor was cooled by passing through a chiller and was then collected in a permeate collection tank.

In the VMD process, the piping and storage tanks were thoroughly insulated and were placed at room temperature. The conductivities were checked with a conductivity meter

(DDSJ-318). The initial conductivity of the simulated wastewater was 358000 μs/cm. Scanning electron microscopy (SEM) of the membrane surface was carried out to investigate the morphology of the scaling layer formed on the membrane. The membrane specimens were stuck to the conductive adhesive carefully and coated with gold before the observations. The membrane distillation flux was then calculated by the following Eq. (21)

$$J = V/At \tag{21}$$

where J is the VMD flux, V is the volume of water cooled by the chiller, A is the effective membrane area, and t is the running time.

4. Results and discussion

4.1 Effect of different operating conditions on permeate water flux

4.1.1 Effect of feed temperature

MD is a temperature-driven process and thus depends on the temperature difference across the membrane. According to Eq. (1), the vapor pressure difference (ΔP) is proportional to water flux. Antoine's equation gives the relation between vapour pressure and temperature and thus the pressure across the membrane is decided by the membrane's surface temperature at the feed and permeate sides. In the VMD process, increasing the feed temperature could significantly raise the membrane's surface temperature in the feed side (T_{fm}), thereby enhancing the permeate water flux. So, the feed temperature is a highly important operating parameter.

In this study, the effect of feed temperature on the permeate water flux of PVDF microporous plate membrane was investigated. Variations in the permeate water flux with feed temperatures at different velocities are shown in Fig. 4. The flux was measured at temperatures from 60 to 85℃ at various velocities (0.032 m/s, 0.048 m/s, 0.064 m/s), while the vacuum degree at the permeate side was maintained constant at 0.085 MPa. It could be seen that there is an exponential increase in the permeate water flux with an increase in the feed temperature. It is due to the exponential relationship between saturated vapor pressure (P_s) and temperature (T_{fm}) on the membrane surface as indicated in Eq. (3), which results in more water vapor molecules penetrating the membrane giving rise to higher water flux. In addition, from these experiments a good agreement is found out between the theoretical and experimental values for the permeate water fluxes.

The TPC and CPC were obtained from Eqs. (12) and (20) based on the calculation of experimental data. Table 3 presents the calculated results obtained at different operating temperatures from 60 to 85 ℃. It indicates that the TPC decreased with an increase in the feed temperature which is opposite to the concentration polarization coefficient. The value of TPC or CPC is closer to 1 implying the presence of less the polarization. Therefore, polarization is intensified leading to lower temperature or higher concentration on the membrane surface which weakens the effect on the permeate water flux with the continuous increase in the feed temperature. The higher is the feed temperature, the greater its effect.

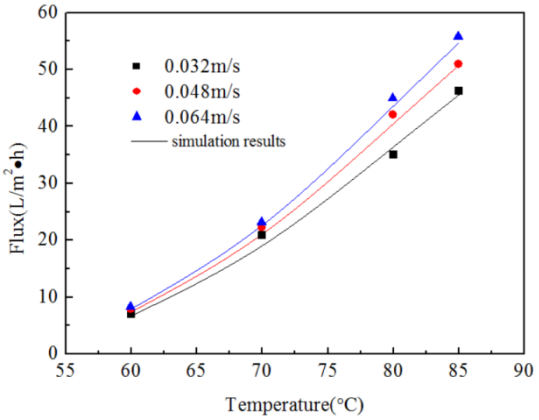

Fig. 4 Variation of flux with temperatures at different feed velocities (vacuum degree, 0.085 MPa)

Table 3 The variation of TPC and CPC at different feed temperatures

Temperature (℃)	Velocity (m/s)	Vacuum degree (MPa)	TPC	CPC
60	0.048	0.085	0.98951	1.07528
70	0.048	0.085	0.97209	1.19868
80	0.048	0.085	0.9504	1.34941
85	0.048	0.085	0.93991	1.42262

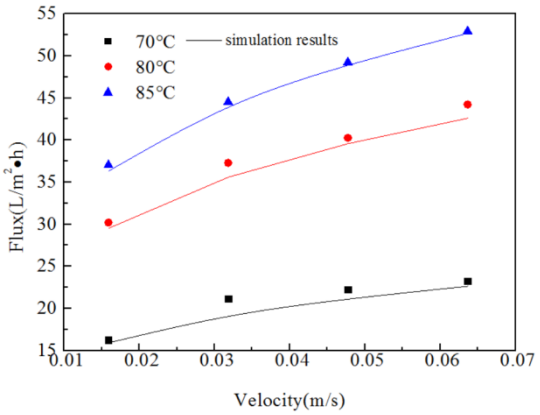

Fig. 5 Variation of flux with feed velocities at different temperatures (at a vacuum degree of 0.085 MPa)

3.1.2 Effect of feed velocity

Feed velocity is one of the most important factors in the operation and performance of VMD. The effect of feed velocity on the permeate water flux was also investigated and the obtained results have been shown in Fig. 5. In this, the feed velocities varied from 0.016 to 0.064 m/s at different temperatures (70℃, 80℃ and 85℃) and at a vacuum degree of 0.085 MPa. It could be seen that the permeate water flux rapidly increases at low velocity, whereas slowly at high velocity with an increase in the feed velocity which may be due to the following.

As indicated in Eq. (10), increasing the feed velocity increases the Reynolds number to enhance the turbulent movement of fluids in the feed side. It reduces the thickness

of heat and mass transfer boundary layer and thus the heat and mass transfer were strengthened. It shows that the effect of TPC and CPC on permeate water flux weakened with an increase in the feed velocity as shown in Table 4. An increase in the TPC leads to higher temperature on the membrane surface. Meanwhile, a higher feed velocity intensifies the shear force on the membrane surface which results in lower CPC, which in turn relatively increases the membrane surface temperature (T_{fm}). Besides, the shortening of residence time increases the feed temperature in the membrane module. On the whole, an increase in the feed temperature and membrane surface temperature (T_{fm}) greatly promote increasing the permeate water flux. However, the concentration on the membrane surface was increased with an increase in the permeate water flux. This could weaken the influence of feed velocity on the polarization phenomenon resulting in a slower increase in the permeate water flux.

3.1.3 Effect of vacuum degree

Safavi (2009) used ANOVA to determine the effect of factors such as temperature, vacuum pressure, flow rate and concentration on the permeate flux. The observed results showed that among the above studied factors vacuum pressure found to be the most significant one. In this study, the effect of vacuum degree on the permeate water flux at different feed temperatures was investigated and the observed results have been illustrated in Fig. 6. It can be seen that there is a linear increase in the permeate water flux with an increase in vacuum degree. Notably, the linear characteristics are maintained even with the changes in the temperatures. This could be due to the following. Based on Eq. (5), increasing the vacuum degree significantly lowers the absolute vapor pressure on the membrane surface at the permeate side. This consequently widens the pressure difference across the membrane (ΔP), keeping P_{fm} as constant. According to Eq. (1), the permeate water flux increased linearly with an increase in ΔP. At the same time, the flux increased from 15.96 to 51.12 L/m^2·h when the vacuum degree varied from 0.060 to 0.090 MPa at a feed temperature of 80 ℃. A large variation in the permeate water flux indicates that vacuum degree is an important contributing parameter in the operation of VMD process. Therefore, the treatment of wastewater with high vacuum degree may effectively increases the permeate water flux.

Table 4 The variation of TPC and CPC at different velocities

Velocity (m/s)	Temperature (℃)	Vacuum degree (MPa)	TPC	CPC
0.016	80	0.085	0.94735	1.37582
0.032	80	0.085	0.94981	1.35549
0.048	80	0.085	0.95137	1.34272
0.064	80	0.085	0.95253	1.33333

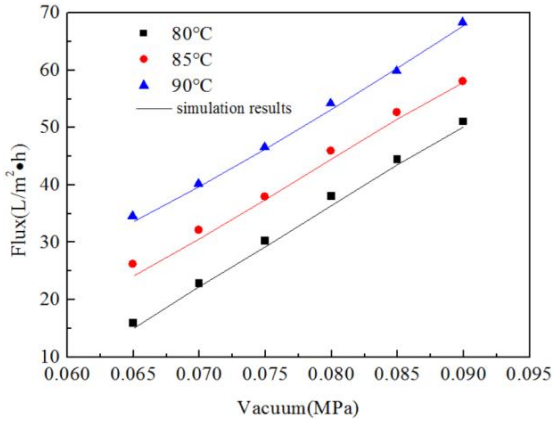

Fig. 6 Variation of flux with vacuum degree at different temperatures (at a feed velocity of 0.048 m/s)

Table 5 The variation of TPC and CPC at different vacuum degrees

Vacuum degree (MPa)	Temperature (℃)	Velocity (m/s)	TPC	CPC
0.065	80	0.048	0.98181	1.11511
0.07	80	0.048	0.97181	1.18396
0.075	80	0.048	0.96325	1.2463
0.08	80	0.048	0.95437	1.31436
0.085	80	0.048	0.94555	1.38571
0.09	80	0.048	0.93745	1.45457

The calculated TPC and CPC data are shown in Table 5. CPC increased significantly with an increase in vacuum degree owing to permeation of more water vapor through the flat membrane which in turn leads to an increase in the concentration on the membrane surface. Thereafter, the boundary layer becomes thickened enhancing the mass transfer resistance which consequently reduces the membrane surface temperature (T_{fm}). The TPC values have shown to decline with an increase in the vacuum degree.

In summary, the operating conditions are critical which influence the performance of VMD significantly. The effects of different operating conditions such as feed temperature, feed velocity and vacuum degree on the permeate water flux were investigated. The observed results showed that with a careful control in the three operating conditions could greatly improve the permeate water flux. However, it is not allowed to enhance the operating conditions without any restriction in order to obtain a higher permeate water flux. Higher feed temperature as well as vacuum degree be capable of enhancing the effect of polarization on the permeate water flux which lead to increasing the mass transfer and heat transfer resistances. Feed velocity may weaken the effect of polarization on the permeate water flux and weakens its influence with an increase in the feed temperature and vacuum degree. Except these operating conditions, concentration is also another important parameter which has an influence and will be discussed in the next section.

3.3 VMD of high-salinity wastewater

Wirth *et al.* (2002) pointed out that the flux decreased less than 30% when the salt concentration increased from 15 to 300 g/L. Thus, the concentration has a profound impact on the permeate water flux. The results of variation of flux with time obtained with real high-salinity wastewater from the resin regeneration is shown in Fig. 7. For this, the operating parameters were maintained as follows: temperature of 75℃, feed velocity of 0.048 m/s

and a vacuum degree of 0.085 MPa. The high-salinity wastewater was simulated and the components of wastewater have been shown in Table 1. It can be seen that the permeate water flux decreased with a change in time (Fig. 7). The maximum permeate water flux of 27 L/m^2·h was obtained under the above-mentioned operating conditions. Also, the curves of permeate water flux versus running time can be divided into two stages: decline stage and sharp decline stage.

For the decline stage, the permeate water flux decreased with the concentration increase from 17 to 25%. The concentration of wastewater increased owing to the removal of water vapor at the vacuum side. However, the molar ratio of water (x_s) and the activity coefficient of water (γ_w)

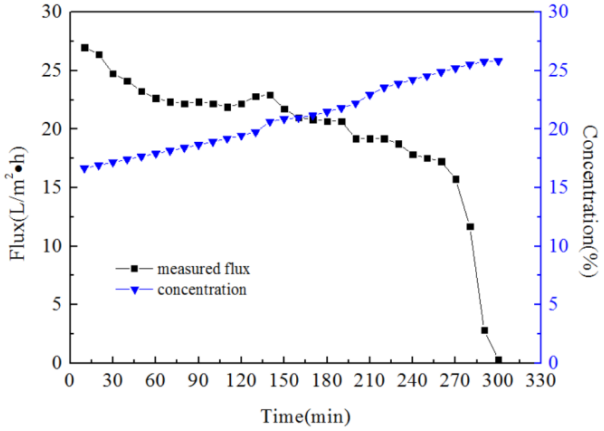

Fig. 7 Variation of permeate flux and concentration with time (temperature 75℃, feed velocity 0.048 m/s, vacuum degree 0.085 MPa)

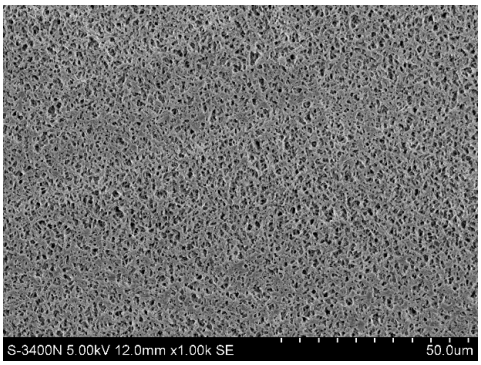

(a) Fresh membrane surface

(b) Deposited membrane surface

Fig. 8 SEM observations on the membrane surface

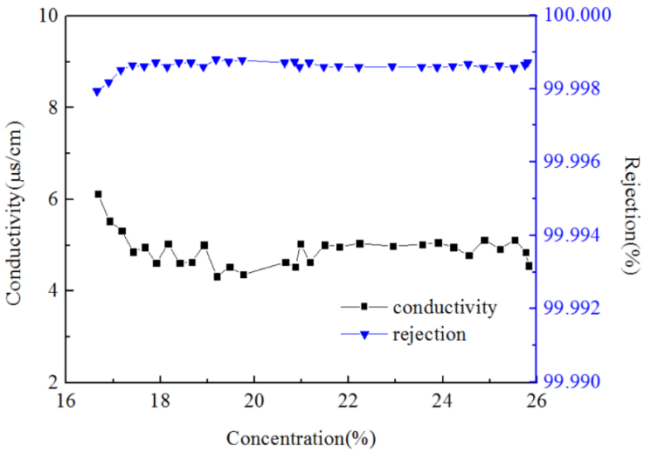

Fig. 9 Variation of conductivity and rejection with concentration (temperature 75℃, feed velocity 0.048 m/s, vacuum degree 0.085 MPa)

decreased with an increase in the concentration of wastewater. In addition, the viscosity (μ) in the feed increased with an increase in the solute concentration. The convective heat transfer in the thermal boundary layer was then enhanced leading to a decrease in the temperature on the membrane surface at the feed side. Thus, the characteristics of feed were changed with an increase in the concentration, which is the probable reason for the observed decline. Besides, the higher concentration polarization led to an increase in the mass transfer resistance in the boundary layer of feed side. The temperature on the membrane surface of the feed side decreased and the saturated vapor pressure on the membrane surface of the feed side correspondingly decreased. Finally, the permeation across the membrane decreased. The time of decline stage was the longest i.e., 260 min and these results indicate that the concentration was not sensitive to the decrease in permeate water flux. When the concentration exceeded 25%, permeate water flux decreased sharply as seen in the sharp decline stage. The value of permeate water flux was almost zero when the concentration was close to 26%. Membrane fouling is also one of the main reasons for the decrease in flux.

Salt crystals formed on the membrane surface are the main sources of membrane fouling. This could be explained through observing the morphology of membrane surface by SEM. SEM images (Fig. 8(b)) indicate that the main deposit on the membrane surface was crystals as compared to the fresh membrane (Fig. 8(a)).

In terms of water quality, Fig. 9 shows the variation in conductivity and rejection with changes in the concentration. Electrical conductivity remains stable at run time and the average value was measured as 4.98 μs/cm. It indicates that the water quality was particularly good as compared to the electrical conductivity of deionized water i.e., 1.9 μs/cm. The rejection ratio is equal to the ratio of electrical conductivity of the permeate water to the feed and was greater than 99.99%. The results show that vacuum membrane distillation is a feasible and effective technique for the treatment of high-salinity wastewater after resin regeneration.

5. Conclusions

In this investigation, VMD was investigated to treat real high-salinity wastewater after resin regeneration. Four factors i.e., feed temperature, velocity, vacuum degree and concentration which affect the performance of VMD were studied. The observed experimental data were in good agreement with the numerical simulation data based on the diffusion model at different operating conditions. The permeation water flux increased with an increase in the operating conditions and decreased with an increase in the concentration. Feed temperature and vacuum degree could enhance the effect of polarization on the permeate water flux which is opposite to velocity. The permeate water flux dropped slightly with time and with concentration varied from 17 to 25%. When the concentration exceeded 25%, permeate water flux decreased sharply and was almost zero when the concentration was close to 26% due to membrane fouling. The average electrical conductivity of permeate water was 4.98 μs/cm. The rejection was greater than 99.99% which was not affected by the concentration. The outcome of this study indicate that VMD is a feasible and an effective treatment technique.

References

Akdemir, E.O. and Ozer, A. (2009), "Investigation of two ultrafiltration membranes for treatment of olive mill wastewaters", *Desalination*, **249**(2), 660-666.

Alkhudhiri, A., Darwish, N. and Hilal, N. (2013), "Treatment of saline solutions using air gap membrane distillation: Experimental study", *Desalination*, **323**, 2-7.

Amali, A.E., Bouguecha, S. and Maalej, M. (2004), "Experimental study of air gap and direct contact membrane distillation configurations: Application to geothermal and seawater desalination", *Desalination*, **168**, 357.

Avlonitis, S.A., Kouroumbas, K. and Vlachakis N. (2003), "Energy consumption and membrane replacement cost for seawater RO desalination plants", *Desalination*, **157**(1), 151-158.

Criscuoli, A., Zhong, J., Figoli, A., Carnevale, M.C., Huang, R. and Drioli, E. (2008), "Treatment of dye solutions by vacuum membrane distillation", *Water Res.*, **42**(20), 5031-5037.

Dao, T. D., Laborie, S. and Cabassud, C. (2016), "Direct As(III) removal from brackish groundwater by vacuum membrane distillation: Effect of organic matter and salts on membrane fouling", *Sep. Purif. Technol.*, **157**, 35-44.

Diban, N., Voinea, O.C., Urtiaga, A. and Ortiz, I. (2009), "Vacuum membrane distillation of the main pear aroma compound: experimental study and mass transfer modeling", *J. Membr. Sci.*, **326**(1), 64-75.

Ducrotoy, J.P. and Elliott, M. (2008), "The science and management of the North Sea and the Baltic Sea: natural history, present threats and future challenges", *Mar. Pollut. Bull.*, **57**(1-5), 8-21.

Edwie, F. and Chung, T.S. (2013), "Development of simultaneous membrane distillation-crystallization (SMDC) technology for treatment of saturated brine", *Chem. Eng. Sci.*, **98**, 160-172.

Garcia-Castello, E., Cassano, A., Criscuoli, A., Conidi, C. and Drioli, E (2010), "Recovery and concentration of polyphenols from olive mill wastewaters by integrated membrane system", *Water Res.*, **44**(13), 3883-3892.

Geng, H., Wu, H., Li, P. and He, Q. (2014), "Study on a new air-gap membrane distillation module for desalination", *Desalination*, **334**(1), 29-38.

Guan, Y., Li, J., Cheng, F., Zhao, J. and Wang, X. (2015), "Influence of salt concentration on DCMD performance for treatment of high salinity NaCl, KCl, $MgCl_2$ and $MgSO_4$ solutions", *Desalination*, **355**, 110-117.

Han, F., Li, W., Yu, F. and Cui, Z. (2014), "Industrial metabolism of chlorine: A case study of a chlor-alkali industrial chain", *Res. Art.*, **21**(9), 5810-5817.

Hickenbottom, K.L. and Cath, T.Y. (2014), "Sustainable operation of membrane distillation for enhancement of mineral recovery from hypersaline solutions", *J. Membr. Sci.*, **454**, 426-435.

Khayet, M., Godino, M.P. and Mengual, J.I. (2003), "Possibility of nuclear desalination through various membrane distillation configurations: A comparative study", *J. Nucl. Desalin.*, **1**(1), 30-46.

Li, N.N., Fane, A.G., Ho, W.S.W. and Matsuura, T. (2008), *Advanced Membrane Technology and Applications*, Wiley, Hoboken, New Jersey, U.S.A.

Martinez, D.L., Florido, D.F.J. and Vazquez, G.M.I. (2000), "Study of polarization phenomena in membrane distillation of aqueous salt solutions", *Separ. Sci. Technol.*, **35**(10), 1485-1501.

Martínez, L. (2004), "Comparison of membrane distillation performance using different feeds", *Desalination*, **168**, 359-365.

Martínez-Díez, L., Florido-Díaz, F.J., and Vázquez-González M.I. (1999), "Study of evaporation efficiency in membrane distillation", *Desalination*, **126** (1-3), 193-198.

Mengual, J.I., Khayet, M. and Godino, M.P. (2004), "Heat and mass transfer in vacuum membrane distillation", *Desalination*, **47**(4), 865-875.

Naidu, G., Choi, Y., Jeong, S., Hwang, T.M. and Vigneswaran, S. (2014), "Experimental and modeling of a vacuum membrane distillation for high saline water", *J. Ind. Eng. Chem.*, **202**, 2174-2183.

Obaidani, S.A., Curcio, E., Macedonio, F., Profio, G.D., Hinai, H.A. and Drioli, E. (2008), "Potential of membrane distillation in seawater desalination: Thermal efficiency, sensitivity study and cost estimation", *J. Membr. Sci.*, **323**(1), 85-98.

Hamza, R.A., Iorhemen, O.T. and Tay, J.H. (2016), "Anaerobic-aerobic granular system for high-strength wastewater treatment in lagoons", *Adv. Environ. Res.*, **5**(3), 169-178.

Safavi, M. and Mohammadi, T. (2009), "High-salinity water desalination using VMD", *Chem. Eng. J.*, **149**(1), 191-195.

Sanmartino, J.A., Khayet, M., García-Payo, M.C., Bakouri, H.E. and Riaza, A. (2016), "Desalination and concentration of saline aqueous solutions up to supersaturation by air gap membrane distillation and crystallization fouling", *Desalination*, **393**, 39-51.

Schofield, R., Fane, A. and Fell, C. (1987), "Heat and mass transfer in membrane distillation", *J. Membr. Sci.*, **33**(3), 299-313.

Sereno, A., Hubinger, M., Comesana, J. and Correa, A. (2011), "Prediction of water activity of osmotic solutions", *J. Food. Eng.*, **49**(2), 103-114.

Singh, D. and Sirkar, K.K. (2012), "Desalination of brine and produced water by direct contact membrane distillation at high temperatures and pressures", *J. Membr. Sci.*, **389**, 380-388.

Sun, Y., Bai, Y., Tian, J.Y., Gao, S.S., Zhao, Z.W. and Cui, F.Y. (2017), "Seawater-driven forward osmosis for direct Treatment of municipal wastewater", *Membr. Water Treat.*, **8**(5), 449-462.

Tomaszewska, M. (1993), "Concentration of the extraction of fluid from sulfuric acid treatment of phosphogypsum by membrane distillation", *J. Membr. Sci.*, **78**(3), 277-282.

Wirth, D. and Cabassud, C. (2002), "Water desalination using membrane distillation: Comparison between inside/out and outside/in permeation", *Desalination*, **147**(1-3), 139-145.

Yun, Y., Ma, R., Zhang, W., Fane, A.G. and Li, J. (2006), "Direct contact membrane distillation mechanism for high concentration NaCl solutions", *Desalination*, **188** (1-3), 251-262.

Zhang, X.M., Guo, Z., Zhang, C.L. and Luan, J.Y., (2016), "Exploration and optimization of two-stage vacuum membrane distillation process for the treatment of saline wastewater produced by natural gas exploitation", *Desalination*, **385**, 117-125.

Zhang, Y., Li, M., Wang, Y., Ji, X., Zhang, L. and Hou, L. (2015), "Simultaneous concentration and detoxification of lignocellulosic hydrolyzates by vacuum membrane distillation coupled with adsorption", *Bioresour*. *Technol*., **197**, 276-283.

Zhao, D., Xue, J., Li, S., Sun, H. and Zhang, Q.D. (2011), "Theoretical analyses of thermal and economical aspects of multi-effect distillation desalination dealing with high-salinity wastewater", *Desalination*, **273**(2), 292-298.

CC

Appendix

Symbols

J	water permeate flux	$L \cdot h^{-1} \cdot m^{-2}$
K	membrane mass transfer coefficient	——
ΔP	vapour pressure difference	kPa
T	temperature	K
P	pressure	kPa
x	molar fraction	——
γ	activity coefficient	——
ε	porosity of the membrane	——
r	radius of pore size	μm
τ	pore tortuosity	——
δ	thickness of membrane	mm
K	knudsen diffusion coefficient	——
M	molecular mass of water	kg/mol
R	gas constant	J/(mol·K)
c	concentration	kg/m^3
k_s	solute mass transfer coefficient	——
d_h	characteristic length	mm
L	channel length	mm
Re	Reynolds number	——
Sc	Sherwood number	——
v	Velocity	m/s
ρ	Density	kg/m^3
μ	viscosity	Pa·s
D	diffusion coefficient	——
Q	quantity of heat	kJ/m^3
h_f	heat transfer coefficient	——
ΔH	latent heat of evaporation	J/mol
C_p	specific heat	kJ/kg/K
k	thermal conductivity	——

Subscripts

fm	membrane surface of the feed	——
pm	membrane surface of the permeate	——
f	the bulk of the feed	——
w	water	——
s	solute	——
v	vacuum side	——
avg	average	——